LETTER | FEBRUARY 11 2026

Enhanced effective nonlinearities in silicon nitride free-standing nanopatterned membranes

P. Franceschini ; M. Nikitin ; A. Tognazzi ; K. Brańko ; O. Takayama ; R. Malureanu ; A. C. Cino ; C. De Angelis ; A. Lavrinenko

APL Photonics 11, 021301 (2026)
https://doi.org/10.1063/5.0309777

Enhanced effective nonlinearities in silicon nitride free-standing nanopatterned membranes

Cite as: APL Photon. 11, 021301 (2026); doi: 10.1063/5.0309777
Submitted: 29 October 2025 • Accepted: 19 January 2026 •
Published Online: 11 February 2026

P. Franceschini,[1,2] M. Nikitin,[3] A. Tognazzi,[2,4,a)] K. Brańko,[5] O. Takayama,[3] R. Malureanu,[3,6] A. C. Cino,[4] C. De Angelis,[1,2] and A. Lavrinenko[3]

AFFILIATIONS

[1] Department of Information Engineering, University of Brescia, via Branze 38, 25123 Brescia, Italy
[2] National Institute of Optics, Consiglio Nazionale delle Ricerche, via Branze 45, 25123 Brescia, Italy
[3] Department of Electrical and Photonics Engineering, Technical University of Denmark, Ørsteds Plads, Building 345A, DK-2800 Kongens Lyngby, Denmark
[4] Dipartimento di Ingegneria, University of Palermo, Viale delle Scienze, Palermo 90128, Italy
[5] Faculty of Physics, University of Warsaw, ul. Pasteura 5, 02-093 Warszawa, Poland
[6] National Centre for Nano Fabrication and Characterization, Technical University of Denmark, Ørsteds plads 347, 2800Kgs. Lyngby, Denmark

[a)] **Author to whom correspondence should be addressed:** andrea.tognazzi@unipa.it

ABSTRACT

Silicon nitride (SiN) represents a promising complementary metal-oxide-semiconductor material for on-chip nanophotonics applications due to its unexpected linear and nonlinear optical properties. Here, we experimentally and numerically investigate the linear and nonlinear response of SiN free-standing nanostructured thin-film membranes. Compared to the unpatterned platform, the design of a square-lattice patterning gives rise to a nonlocal resonant mode that enhances the effective third-order optical nonlinearity by a factor of 3.4–5 at the resonance wavelength, as determined from Z-scan experiments. Finite-element simulations clarify that the magnitude of the lattice-induced frequency dispersion of the Kerr coefficient also depends on the spectral and geometrical properties of the interacting light excitation. Our results propose patterned SiN nanomembranes as a promising nanophotonics platform for enhanced nonlinear frequency conversion processes.

The development of efficient methods for nonlinear (NL) frequency conversion represents one of the most active fields of present research. Since the pioneering experiments on second-harmonic generation,[1] various platforms hosting NL frequency mixing processes have been employed to maximize the intensity of the output radiation, which can be described by the relation[2,3] $I_{NL}(n\omega) \propto \left\{\chi^{(n)}\,[E_{FF}(\omega)]^n\,L_{int}\right\}^2$, where $\chi^{(n)}$ is the nth order NL coefficient, $E_{FF}(\omega)$ is the electric field at fundamental frequency ω, and L_{int} is the interaction length. Although being the fundamental building block for near-infrared to visible (NIR-to-VIS) frequency conversion due to their large bulk NL coefficient $\chi^{(n)}_{bulk}$, conventional NL crystals (like BBO) suffer from strong absorption in the vacuum ultraviolet (VUV) spectral range (in addition to inherently short L_{int}), thus preventing efficient VIS-to-VUV generation.[3] These limitations have been partially overcome by the use of dielectric metasurfaces, optical devices consisting of engineered distributions of low-loss nano-resonators. By a suitable design of the geometrical parameters, the electric field of the pump excitation can be strongly confined inside the resonator (i.e., resonant mode), thus allowing the efficient access to the bulk nonlinearity of the constituent material. In this sense, the presence of the resonant mode effectively increases, by some factor f, the NL coefficient $\chi^{(n)} = f \cdot \chi^{(n)}_{bulk}$. However, the substrate—which, from a structural point of view, is the supporting constituent of the metasurface—may limit the intensity of the input pump field $E_{FF}(\omega)$ due to self-phase modulation in the case of backside illumination (i.e., when the fundamental frequency beam excites the nano-resonators after propagating through the

substrate).[3] Recently, it has been demonstrated that these limitations in terms of L_{int} and maximum $E_{FF}(\omega)$ can be overcome by employing free-standing dielectric thin films (membranes), with thickness comparable to the coherence length, for NL mixing processes.[3] Moreover, the intensity I_{NL} can be further increased by exploiting nonlocal (i.e., extended) resonant modes of the electromagnetic field arising when the membranes feature a patterned structure. This has recently been demonstrated for γ-Al_2O_3-based photonic crystal nanomembranes featuring a square periodic lattice of circular holes.[4] Within the framework of integrated nanophotonics, the need for a complementary metal-oxide-semiconductor (CMOS)-compatible material with large third-order optical nonlinearity is crucial for applications such as all-optical processing, computing, switching, and communications.[5–7] Traditionally, silicon (Si) represents the principal constituent of silicon-on-insulator platforms due to its large Kerr nonlinearity, high refractive index, and low losses in the visible spectral range. However, its relatively narrow bandgap ($E_g \simeq 1.1$ eV) limits its functions and applications at UV to VIS and NIR wavelengths. Recently, silicon nitride (SiN) has gathered increasing interest as a promising alternative[7] for its ease of incorporation and processing, broadband transparency ($E_g \simeq 4$ eV[8,9]), relatively high refractive index, and intrinsically large nonlinear refractive index, which can be beneficial for many on-chip nanophotonics applications, such as third-harmonic generation (THG),[7] optical parametric oscillation,[5] and supercontinuum generation.[10,11] While intrinsic third-order nonlinearities in SiN-based thin films and free-standing membranes has been widely reported, the study of their enhancement due to nonlocal modes have been less investigated (to the best of our knowledge, a comprehensive theoretical analysis of the THG in such membranes has been published very recently[12]).

In this letter, we report on the enhancement of the effective third-order optical nonlinearity in free-standing SiN membranes arising from the presence of a lattice resonance. Starting from unpatterned 50-nm-thick free-standing membranes, we design a two-dimensional periodic nano-patterned structure inducing a lattice resonance (LR) at 750 nm wavelength. Linear optical properties of the fabricated sample have been experimentally and numerically studied. The optical nonlinearity was experimentally investigated by the Z-scan technique, performed at the resonance wavelength, whose results show an enhancement of the effective NL refractive index n_2 and absorption coefficient β in the case of the patterned membrane compared to the pristine one. The post-processing of the experimental data, combined with time-domain and frequency-domain modeling, allowed us to identify and quantify how the spectral and geometrical properties of the light excitation interacting with the structure affect the magnitude of the enhancement factor (f).

A sketch of the structure under analysis is shown in Fig. 1(a). The membrane consists of a SiN slab (with thickness $t = 50$ nm) patterned with a square array (period Λ) of circular holes (diameter ϕ). As shown by the design procedure detailed in Ref. 12, the patterned membrane is capable of supporting resonant modes with different natures in the VIS–NIR spectral region. In particular, we designed the metasurface to support a lattice resonance mode in the 750–800 nm spectral range by a suitable optimization of the geometrical parameter Λ. In view of applications involving nonlinear processes, the leaky nature of the selected resonance ensures

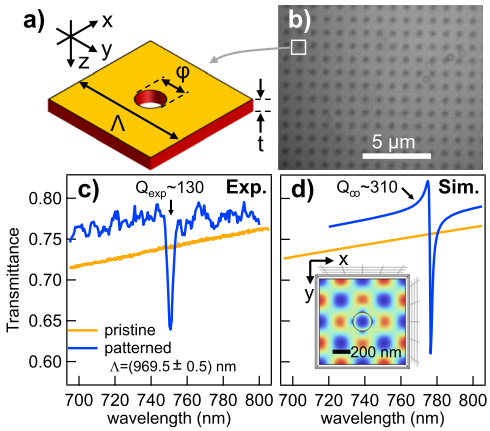

FIG. 1. Design and linear properties. (a) Design of the unit cell. Geometrical parameters: period Λ, thickness t, and hole diameter ϕ. (b) Image of the fabricated metasurface (top view, optical microscope). (c) Measured linear transmittance spectra of the pristine (unpatterned, yellow line) and patterned (blue line) membrane. (d) Calculated linear transmittance spectra of the pristine (yellow line) and patterned (blue line) metasurface. The inset shows the electric field distribution (absolute value) at resonance.

proper coupling to an external pump radiation, and the designed wavelength well matches the most common table-top laser systems. Moreover, given the geometry of the unit cell, the field distribution of the resonance was optimized to maximize its localization in the region occupied by SiN (which acts as a nonlinear material), as performed previously.[13,14] The membranes were fabricated[15] on a Si wafer with a SiN layer deposited using low-pressure chemical vapor deposition (LPCVD) techniques. The patterning was defined by electron beam lithography (EBL) and subsequent SiN etch. On the backside, we used aligned UV lithography, SiN, and Si etch to obtain free-standing membranes. Non-patterned (pristine) membranes were prepared in the same batches as references (see the supplementary material, Sec. S1). Ellipsometry measurements performed on fabricated samples provide $t = 53.0$ nm and $t = 49.4$ nm for pristine and patterned [Fig. 1(b)] membranes, respectively, and the analysis of the scanning electron microscopy (SEM) images gives $\phi = 200$ nm (see the supplementary material, Sec. S2).

The linear optical properties of the fabricated samples were measured in the VIS–NIR spectral region as detailed in the supplementary material, Sec. S3A. Figure 1(c) shows the measured linear transmittance spectrum (normal incidence) of the pristine and patterned membrane (yellow and blue solid lines, respectively), the latter featuring $\Lambda = (969.5 \pm 0.5)$ nm (retrieved from the analysis of the optical microscope image) and exhibiting a spectral feature at 750 nm. Additional data for membranes with different values of Λ are reported in the supplementary material, Sec. S5A. Using as inputs the values of the geometrical parameters retrieved from SEM and the SiN refractive index taken from Ref. 9 ($n_{SiN} = 2$, $k_{SiN} = 0$), we performed frequency-domain numerical simulations (Comsol) of the linear transmittance of the pristine and patterned samples, and the results are displayed in Fig. 1(d), where the inset shows the numerically calculated field distribution at resonance wavelength. Based on the numerical results, we ascribe the spectral feature

probed at $\lambda_{LR} \sim 750$ nm wavelength in Figs. 1(c)–1(a) LR, which manifests itself in the form of a Fano resonance.[16,17] The nonlocal nature of the resonance under analysis is further confirmed by the measured and calculated dependence of λ_{LR} on Λ, as detailed in the supplementary material, Secs. S5A and S7A. By fitting a theoretical Fano line shape[16] to the experimental data (see the supplementary material, Sec. S5A), the value of the resonance quality factor (Q) probed in the experiment is estimated as $Q_{\mathrm{exp}} \sim 130$, which is lower than the calculated one $Q_\infty \sim 310$ ($Q = \lambda_r/\gamma$, with λ_r and γ being the spectral position and bandwidth of the resonance, respectively). Discrepancies in the width and amplitude of the LR profile in the measured and calculated spectra can be ascribed mainly to finite-size effects (which result in a non-optimal excitation of the resonance) since, from a geometrical point of view, the structure under analysis consists of a two-dimensional periodic repetition of a unit cell.

In order to better investigate the effect of the finite-size nature of the patterning on the appearance of the LR spectral feature, we performed time-domain numerical simulations (Tidy3D) of the linear optical properties in the case of membranes featuring a two-dimensional square patterning with limited spatial extension. Figure 2(a) shows the linear transmittance spectra for finite-size patterned membranes composed of a total number N^2 of unit cells, where N denotes the number of unit cells along one direction of the square patterning. Clearly, the bandwidth of the spectral feature decreases with increasing N. This aspect can be better visualized by looking at the corresponding value of the Q-factor, displayed in Fig. 2(b), which shows that a finite-size metasurface exhibits a lower value of Q compared to the infinitely periodic one ($Q_\infty \sim 310$). Our analysis, in line with other studies on periodic structures,[18] confirms that finite-size effects result in a non-optimal excitation of the resonance due to the collective nature of the LR.

The third-order optical nonlinearity of pristine and patterned membranes has been investigated by the Z-scan technique (see inset in Fig. 3(a)),[19,20] by employing a pulsed excitation radiation with central wavelength $\lambda_0 = 750$ nm, spectral bandwidth (full-width at half maximum) $\Delta\lambda = 35$ nm, and featuring a beam waist at focus $w_0 = (19.8 \pm 0.3)$ μm. Closed and open aperture (CA and OA, respectively) traces have been measured by recording the fraction of incident light transmitted by the sample for various positions

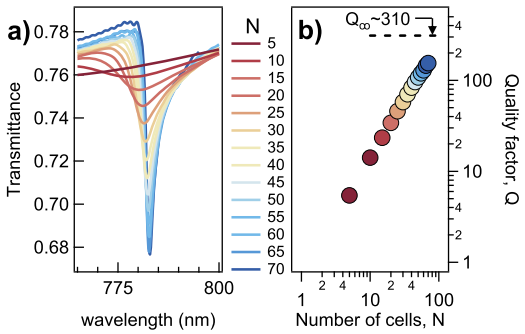

FIG. 2. Finite-size metasurface. (a) Calculated transmittance spectra for a square finite-size metasurface featuring N unit cells along one side. (b) Q-factor as a function of the number of cells N retrieved from the spectra in panel a. The dotted black line at $Q_\infty = 310$ denotes the value for an infinitely periodic metasurface ($N \to \infty$).

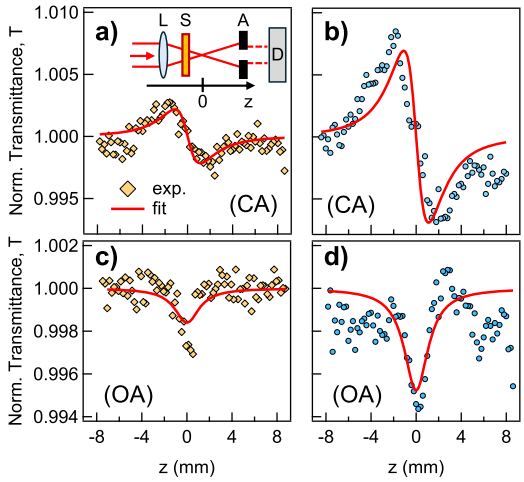

FIG. 3. Z-scan Traces. (a, b) Closed and (c, d) open aperture Z-scan data for free-standing (a, c) pristine and (b, d) patterned SiN membranes with $I_0 = 720$ GW/cm^2 (a, b), $I_0 = 1017$ GW/cm^2 (c), and $I_0 = 650$ GW/cm^2 (d). A theoretical profile (red solid line) based on Ref. 19 has been fitted to the measured data (markers). The inset sketches the Z-scan setup. The position $z = 0$ denotes the beam focus. L: lens; S: sample; A: aperture; D: detector. The data in (a) and (b) have been measured with $S = 0.495$ and $S = 0.485$, respectively.

along the propagation axis (z-axis; see the supplementary material, Sec. S3B). First, we focused our attention on the NL refractive index n_2. For this purpose, we measured CA Z-scan traces for both samples, whose results are displayed in Figs. 3(a) and 3(b) (pristine and patterned membranes, respectively). The CA traces feature a peak–valley (p–v) configuration (consistent with previous reports on SiN[8,21]), thus denoting a self-defocusing effect described in terms of a negative-valued n_2. As expected, in the case of the patterned membrane, the value of ΔT_{p-v}, the difference between the normalized peak and valley transmittance, $T_p - T_v$, is larger in amplitude compared to the pristine one. Since the two measurements displayed in Figs. 3(a) and 3(b) have been taken by employing the same value of irradiance I_0, the difference in ΔT_{p-v} suggests an enhanced value of the effective n_2 coefficient of the patterned membrane compared to the pristine one. The retrieved value of the NL refractive index (see the supplementary material, Sec. S5B) for the pristine membrane is $n_2^{pri} = -3.8 \times 10^{-18}$ m^2/W [Fig. 3(a)], which is consistent with previously reported values on SiN.[22,23] On the other hand, in the case of the patterned membrane [Fig. 3(b)], $n_2^{pa} = -1.3 \times 10^{-17}$ m^2/W, which is 3.4 times larger than n_2^{pri}. We ascribe the enhancement of the value of effective n_2 to the larger field confinement occurring at the LR. The values of the coefficients retrieved from the analysis are summarized in Table I. The value of n_2^{pa} is confirmed by the

TABLE I. Nonlinear parameters n_2 and β retrieved from the analysis of Z-scan traces (excitation wavelength $\lambda_0 = 750$ nm).

	Pristine	Patterned	f
n_2 $[10^{-18}$ m^2/W$]$	−3.8	−13	3.4
β $[10^{-12}$ m/W$]$	9.4	47	5

repetition of the measurement at the same and lower irradiance values (see the supplementary material, Sec. S4A). Then, we turned our attention to the NL absorption coefficient β; therefore, we measured OA Z-scan traces for both samples. The data displayed in Figs. 3(c) and 3(d) (pristine and patterned sample, respectively) show the characteristic NL absorption dip. The analysis on the OA traces (see the supplementary material, Sec. S5B) provides a value of the NL absorption coefficient of $\beta^{pri} = -9.4 \times 10^{-12}$ m/W and $\beta^{pa} = -4.7 \times 10^{-11}$ m/W (pristine and patterned sample, respectively), which suggests a similar value of the enhancement factor ($f \sim 5$).

Based on these results, we ascribe the amplitude of the probed f parameter of the optical nonlinearity to two main aspects. First, we consider the effect of the ratio between the LR bandwidth γ and the bandwidth of the excitation laser pulse on the output of a third-order NL process. In particular, since the physics involved in a Z-scan experiment can be described in terms of a four-wave mixing process $\chi^{(3)}(\omega, \omega, -\omega; \omega)$, we refer to the analysis provided in Ref. 12 regarding THG enhancement occurring in patterned SiN membranes. As detailed in Ref. 12, in the case of a pulsed excitation with a pulse duration of $\tau_p \sim 24$ fs (i.e., the transform-limited pulse duration value corresponding to $\Delta\lambda = 35$ nm), the enhancement of the THG due to the LR, occurring in an infinitely two-dimensional periodic patterned membrane, is $\eta_{THG} = 20$. This result sets a threshold in the maximum achievable enhancement due to the smaller bandwidth of the LR compared to the laser excitation. However, a second aspect should be taken into account, and it is related to finite-size effects. As mentioned previously, the finite nature of the illumination/structure may prevent a complete excitation of the resonance, thus resulting in an effectively lower Q-factor. Within the context of a third-order NL process, for which the output signal intensity scales as the third power of the Q-factor at fundamental frequency ($P_{3\omega} \propto Q_{FF}^3$[24]), finite-size effects become more crucial. To better understand this point, it is useful to recall that, from an experimental point of view, in the Z-scan experiment, the sample moves along the propagation direction (z-axis) of a focused beam. Therefore, the number of unit cells illuminated by the laser spot changes as the sample moves along z. In particular, the number of illuminated cells is large when the sample is far away from the focus, and it decreases to a minimum as the focus is reached. Therefore, the level of excitation of the LR changes as the sample position varies, and so does the value of the Q-factor ascribed to the finite-size region optically excited. In order to provide an estimation of the effective value of the Q-factor probed in the NL experiment, it is possible to interpret a Z-scan trace obtained for the patterned membrane as the *average* response of the electric field confinement due to the LR. Therefore, by assuming an effective number of illuminated cells of $N_{eff} \simeq 66$ (see the supplementary material, Sec. S5C), the corresponding value of the Q-factor is $Q_{\langle N \rangle} \sim 150$, obtained from the numerical results in Fig. 2(b). Therefore, the correction term due to the finite-size effect can be estimated as $\eta_{FS} = \left(Q_{\langle N \rangle}/Q_\infty\right)^3 = (150/310)^3 \simeq 0.113$ (since a third-order process is involved). Finally, taking into account both spectral bandwidth and finite-size effects, the resulting theoretical f parameter can be estimated as $f^{theo} = \eta_{THG} \cdot \eta_{FS} \simeq 2.3$, which is compatible with the value retrieved from Z-scan experiments ($f^{\exp} \sim 3.4 - 5$). In order to include the effect of absorption (abs) losses, we numerically calculated the transmittance spectra by assuming a nonzero imaginary component of the refractive index of SiN (k_{SiN}), as suggested by previous studies[14] (see the supplementary material, Sec. S7B for more details). By assuming $k_{\mathrm{SiN}} = 0.01$, we obtained $Q_\infty^{abs} \sim 74$ and $Q_{\langle N \rangle}^{abs} \sim 55$. Therefore, in the case of optical losses, the estimation of the magnitude of the enhancement factor gives $f_{abs}^{theo} = \eta_{THG} \cdot \eta_{FS}^{abs} = \eta_{THG} \cdot \left(Q_{\langle N \rangle}^{abs}/Q_\infty^{abs}\right)^3 = 8.2$; therefore, the presence of optical losses contributes to increasing the magnitude of the enhancement factor (still compatible with the value retrieved with the Z-scan experiments). Our evaluation of the enhancement factor f^{theo} does not include the contribution due to the superposition of multiple wave vector components in the focused light (originating from the presence of the focusing lens in the Z-scan setup) since, under our experimental conditions, the modulation of the Q-factor due to out-of-normal incidence can be neglected (see the supplementary material, Sec. S7C for additional details). Qualitatively, the meaning of the enhancement factor f considered in this study can be interpreted by recalling that the Z-scan measurement probes the effect of the NL polarization in the *far-field* region of the space. The latter quantity includes various contributions originating from different NL mixing processes—each one ascribed to a specific element of the bulk $\chi_{bulk}^{(3)}$ tensor—triggered by the localized field distribution in the *near-field* region. In this sense, an observer in the far-field can model[25] the system response via an effective $\chi_{eff}^{(3)}$ tensor, where each element of $\chi_{eff}^{(3)}$ includes the contributions from various $\chi_{bulk}^{(3)}$ terms, which are summarized by f. In line with previous studies in the context of photonic crystals,[26–28] the analysis has been complemented by the investigation of metasurfaces featuring elliptical holes in the unit cell. Compared to the circular shape, the elliptical one determines polarization dependent effects, but it does not introduce appreciable variations on the magnitude of the enhancement factor (see the supplementary material, Sec. S7D for additional details). In summary, we fabricated pristine and patterned free-standing SiN membranes, the latter designed to exhibit a lattice resonant nonlocal mode. The measured linear optical properties of the fabricated samples have been numerically investigated to confirm the nature of the probed resonant mode. The NL refractive index n_2 and absorption coefficient β have been determined by the Z-scan method at a wavelength of 750 nm. The magnitude of enhancement of the third-order optical nonlinearity originated by the LR-induced field confinement has been numerically addressed, taking into account the influence of the laser spectral bandwidth and finite-size effects. The results suggest the potential application of square-lattice patterned SiN membranes in integrated photonics devices and potential constraints in the enhancement.

The supplementary material includes fabrication details, SEM images of fabricated samples, a scheme of the Z-scan setup, details of beam spatial characterization for Z-scan, additional experimental closed-aperture traces, additional linear transmittance spectra, analysis of linear transmittance spectra, details of the theoretical model for closed- and open-aperture traces, the theoretical model for the effective number of illuminated unit cells, additional notes

for numerical simulations, and additional numerical simulations for varying lattice periods.

A. T. acknowledges financial support from the University of Palermo through "Fondo Finalizzato alla Ricerca di Ateneo 2025 (FFR2025)". A. C. C. aknowledges Ecosistema dell'Innovazione Sicilian MicronanoTech Research And Innovation Center - SAMOTHRACE - B73C22000810001- ECS_00000022. C.D.A. acknowledges financial support from the European Union under the Italian National Recovery and Resilience Plan (NRRP) of NextGenerationEU, in partnership on "Telecommunications of the Future" (PE00000001 – program "RESTART"), PNRR RESTART Project SMART METASURFACES ADVANCING RADIO TECHNOLOGY – SMART – CUP E63C22002040007. C.D.A. acknowledges financial support from the NATO Project "MELITE" (SPS Grant No. G6137). A.L. acknowledges financial support from Villum Fonden (No. 00037822). O.T. acknowledges financial support from Novo Nordisk Fonden, Project Grant in Natural and Technical Sciences, "Extremely anisotropic nanostructures for lightwave steering" (Extra Light, grant No. 0093187).

AUTHOR DECLARATIONS

Conflict of Interest

The authors have no conflicts to disclose.

Author Contributions

P. Franceschini and M. Nikitin contributed equally to this study.

P. Franceschini: Data curation (equal); Investigation (lead); Methodology (supporting); Software (equal); Visualization (lead); Writing – original draft (lead); Writing – review & editing (equal). **M. Nikitin**: Data curation (equal); Investigation (lead); Resources (lead); Writing – review & editing (equal). **A. Tognazzi**: Data curation (equal); Funding acquisition (equal); Investigation (equal); Methodology (equal); Software (equal); Writing – original draft (equal); Writing – review & editing (equal). **K. Brańko**: Data curation (equal); Investigation (equal); Writing – review & editing (equal). **O. Takayama**: Data curation (equal); Funding acquisition (equal); Investigation (equal); Writing – review & editing (equal). **R. Malureanu**: Data curation (equal); Investigation (equal); Resources (supporting); Writing – review & editing (equal). **A. C. Cino**: Resources (equal); Supervision (equal); Writing – review & editing (equal). **C. De Angelis**: Funding acquisition (equal); Project administration (equal); Resources (equal); Supervision (equal); Writing – review & editing (equal). **A. Lavrinenko**: Conceptualization (lead); Funding acquisition (equal); Project administration (equal); Resources (equal); Supervision (equal); Writing – review & editing (equal).

DATA AVAILABILITY

The data that support the findings of this study are available within the article and its supplementary material. The notebook of Tidy3D code is available online in https://www.flexcompute.com/tidy3d/EGMXrFOavk.

REFERENCES

[1] P. A. Franken, A. E. Hill, C. W. Peters, and G. Weinreich, "Generation of optical harmonics," Phys. Rev. Lett. **7**, 118–119 (1961).
[2] R. Boyd, *Nonlinear Optics* (Academic Press, Cambridge, MA, USA, 2002).
[3] K. Konishi, D. Akai, Y. Mita, M. Ishida, J. Yumoto, and M. Kuwata-Gonokami, "Tunable third harmonic generation in the vacuum ultraviolet region using dielectric nanomembranes," APL Photonics **5**, 066103 (2020).
[4] K. Konishi, D. Akai, Y. Mita, M. Ishida, J. Yumoto, and M. Kuwata-Gonokami, "Circularly polarized vacuum ultraviolet coherent light generation using a square lattice photonic crystal nanomembrane," Optica **7**, 855–863 (2020).
[5] J. S. Levy, A. Gondarenko, M. A. Foster, A. C. Turner-Foster, A. L. Gaeta, and M. Lipson, "CMOS-compatible multiple-wavelength oscillator for on-chip optical interconnects," Nat. Photonics **4**, 37 (2010).
[6] G.-R. Lin, S.-P. Su, C.-L. Wu, Y.-H. Lin, B.-J. Huang, H.-Y. Wang, C.-T. Tsai, C.-I. Wu, and Y.-C. Chi, "Si-rich SiN_x based Kerr switch enables optical data conversion up to 12 Gbit/s," Sci. Rep. **5**, 9611 (2015).
[7] D. J. Moss, R. Morandotti, A. L. Gaeta, and M. Lipson, "New CMOS-compatible platforms based on silicon nitride and Hydex for nonlinear optics," Nat. Photonics **7**, 597 (2013).
[8] B. Ding, X. Yu, H. Lu, X. Xiu, C. Zhang, C. Yang, S. Jiang, B. Man, T. Ning, and Y. Huo, "Third-order optical nonlinearity in silicon nitride films prepared using magnetron sputtering and application for optical bistability," J. Appl. Phys. **125**, 113102 (2019).
[9] L. Y. Beliaev, E. Shkondin, A. V. Lavrinenko, and O. Takayama, "Optical, structural and composition properties of silicon nitride films deposited by reactive radio-frequency sputtering, low pressure and plasma-enhanced chemical vapor deposition," Thin Solid Films **763**, 139568 (2022).
[10] A. Klenner, A. S. Mayer, A. R. Johnson, K. Luke, M. R. E. Lamont, Y. Okawachi, M. Lipson, A. L. Gaeta, and U. Keller, "Gigahertz frequency comb offset stabilization based on supercontinuum generation in silicon nitride waveguides," Opt. Express **24**, 11043–11053 (2016).
[11] D. R. Carlson, D. D. Hickstein, A. Lind, S. Droste, D. Westly, N. Nader, I. Coddington, N. R. Newbury, K. Srinivasan, S. A. Diddams, and S. B. Papp, "Self-referenced frequency combs using high-efficiency silicon-nitride waveguides," Opt. Lett. **42**, 2314–2317 (2017).
[12] M. Nikitin, K. Nijsen, A. Moltke, O. Takayama, R. Malureanu, O. Bang, and A. V. Lavrinenko, "Third-harmonic generation of ultraviolet light in silicon nitride metasurface: A numerical study of pulse duration dependence," Opt. Express **33**, 17693–17704 (2025).
[13] L. Qu, L. Bai, C. Jin, Q. Liu, W. Wu, B. Gao, J. Li, W. Cai, M. Ren, and J. Xu, "Giant second harmonic generation from membrane metasurfaces," Nano Lett. **22**, 9652 (2022).
[14] L. Li, L. Qu, W. Wu, C. Li, L. Bai, C. Wang, Z. Guo, P. Zhu, X. Liu, W. Cai, M. Ren, and J. Xu, "Optimizing second harmonic generation in metasurfaces: The mode overlap factor," Laser Photonics Rev. **2025**, e01098 (2025).
[15] M. Nikitin, O. Takayama, R. Malureanu, and A. Lavrinenko, "On the use of membrane metasurfaces for high-efficiency third harmonic generation," in Proceedings of 24th International Conference on Transparent Optical Networks (IEEE, 2024).
[16] U. Fano, "Effects of configuration interaction on intensities and phase shifts," Phys. Rev. **124**, 1866–1878 (1961).
[17] M. F. Limonov, M. V. Rybin, A. N. Poddubny, and Y. S. Kivshar, "Fano resonances in photonics," Nat. Photonics **11**, 543 (2017).
[18] J. O. Grepstad, M. M. Greve, B. Holst, I.-R. Johansen, O. Solgaard, and A. Sudbø, "Finite-size limitations on quality factor of guided resonance modes in 2D photonic crystals," Opt. Express **21**, 23640–23654 (2013).
[19] M. Sheik-Bahae, A. A. Said, T.-H. Wei, D. J. Hagan, and E. W. Van Stryland, "Sensitive measurement of optical nonlinearities using a single beam," IEEE J. Quant. Electron. **26**, 760–769 (1990).
[20] A. Tognazzi, P. Franceschini, T. N. L. Tran, A. Chiasera, M. A. Vincenti, A. C. Cino, N. Akozbek, M. Scalora, and C. De Angelis, "Z-Scan theory for thin film measurements: Validation of a model beyond the standard approach using ITO and HfO_2," Opt. Mater. X **19**, 100242 (2023).

[21] S. Bej, N. Tkachenko, R. Fickler, and T. Niemi, "Ultrafast modulation of guided-mode resonance in a nonlinear silicon nitride grating," Adv. Opt. Mater. **13**, 2402632 (2025).
[22] K. Ikeda, R. E. Saperstein, N. Alic, and Y. Fainman, "Thermal and Kerr nonlinear properties of plasma-deposited silicon nitride/silicon dioxide waveguides," Opt. Express **16**, 12987–12994 (2008).
[23] C. J. Krückel, A. Fülöp, Z. Ye, P. A. Andrekson, and V. Torres-Company, "Optical bandgap engineering in nonlinear silicon nitride waveguides," Opt. Express **25**, 15370–15380 (2017).
[24] K. Koshelev, Y. Tang, K. Li, D.-Y. Choi, G. Li, and Y. Kivshar, "Nonlinear metasurfaces governed by bound states in the continuum," ACS Photonics **6**, 1639 (2019).
[25] U. Arregui Leon, L. Carletti, D. Rocco, C. De Angelis, and G. Della Valle, "Thz generation via optical rectification in nanomaterials: Universal modeling approach and effective $\bar{\bar{\chi}}^{(2)}$," Laser Photonics Rev. **18**, 2300669 (2024).
[26] M. J. Steel and R. M. Osgood, "Elliptical-hole photonic crystal fibers," Opt. Lett. **26**, 229–231 (2001).
[27] M. J. Steel and R. M. Osgood, "Polarization and dispersive properties of elliptical-hole photonic crystal fibers," J. Lightwave Technol. **19**, 495 (2001).
[28] L. Huang, J. Zhou, F. Sun, Z. Fu, and H. Tian, "Optimization of one dimensional photonic crystal elliptical-hole low-index mode nanobeam cavities for on-chip sensing," J. Lightwave Technol. **34**, 3496–3502 (2016).